Journal of Air Pollution and Health (Autumn 2020); 5(4): 233-242

Original Article

Available online at http://japh.tums.ac.ir

# Numerical simulation of photocatalytic oxidation of gaseous pollutants using low Reynolds number turbulence models

*Shijian Peng, Bensheng Zhao, Haiyan Zhang, Jia Wang, Baoqing Deng**

Department of Environmental Science and Engineering, University of Shanghai for Science and Technology, Shanghai 200093, P R China

ARTICLE INFORMATION

*Article Chronology:*
Received 29 October 2020
Revised 27 November 2020
Accepted 19 December 2020
Published 30 December 2020

*Keywords:*
Photocatalytic oxidation; CFD; Degradation efficiency

CORRESPONDING AUTHOR:

bqdeng@usst.edu.cn
Tel: 00862155271991
Fax: 008655271991

ABSTRACT

**Introduction:** Photocatalytic oxidation of gaseous pollutants in differential reactors is simulated using computational fluid dynamics.

**Materials and methods:** The momentum equation and pollutant transport are solved by using ANSYS Fluent. The SIMPLE algorithm is used to treat the pressure-velocity coupling. The laminar flow and low Reynolds k−ε models are used to describe turbulence.

**Results:** Velocity field distribution and degradation efficiency of different models at various flow rates were obtained and compared with the experimental data. The simulation results of degradation efficiency under different models are basically consistent.

**Conclusion:** Although low Reynolds k-ε models have better simulation results for high inlet flow rates, in terms of computation complexity, laminar flow is recommended for simulation.

## Introduction

Photocatalytic oxidation technology has attracted significant attention in the field of pollutant control [1, 2]. Under the illumination of UV light, photocatalytic reaction is activated through the absorption of photons with the energy greater than the band-gap energy, producing an electron–hole pair [3–5]. A series of reduction and oxidation reactions are followed transforming pollutants into carbon dioxide and water.

Hydrodynamics plays an important role in photocatalytic reaction, which directly influences the transport of pollutants within the reactor. An effective methodology to understand the hydrodynamics is computational fluid dynamics (CFD), in which the continuity and momentum equations are usually solved by using finite volume method. Annular reactors with simple geometry have been successfully simulated with laminar flow [6–8] and turbulent flow [9, 10]. For reactors with multiple lamps or complex catalyst surface, CFD simulations depict good ability adapting to complex internal configurations under the laminar flow [11–13]. When the catalyst exists as particles, multiphase flow was simulated in reactors in combination with suitable turbulence models [14–18]. In general, good agreement was obtained between the experimental data and the simulations for these laboratory-scale reactors.

When simulating the photocatalytic reaction in

Please cite this article as: Peng Sh, Zhao B, Zhang H, Wang J, Deng B. Numerical simulation of photocatalytic oxidation of gaseous pollutants using low Reynolds number turbulence models. Journal of Air Pollution and Health. 2020; 5(4): 233-242.

laboratory scale reactors, the kinetic rate equation must be known, which is usually described by the Langmuir-Hinshelwood equation. The rate constants in the Langmuir-Hinshelwood equation are measured in differential reactors [6, 19–22]. Differential reactors are very small and contains a plane surface coated with the catalyst. By using the assumption of perfect mixing, the rate constants can be obtained from the experiment in differential reactors [19, 22]. On the other hand, laminar flow [23] or turbulent flow [20] were also used to simulate differential reactors and evaluate rate constants. However, no assessment on the effect of laminar and turbulent flows was conducted.

The simulation of differential reactors is crucial to determine the rate constants. In this work, laminar flow and several low-Re $k-\varepsilon$ turbulence models are used to simulate a differential reactor. The aim is to determine the suitable model for the evaluation of rate constants of photocatalytic reactions in differential reactors.

## Materials and methods

### *Flow equations*

For the photocatalytic reaction in differential reactors, the air is usually used as carrier gas. Air flow in the reactor obeys the conservation law of mass and momentum. The aim of differential reactors is to measure the reaction rate. Therefore, air flow is usually maintained at steady state. Under the steady condition, the continuity equation and Navies-Stokes equation can be written as follows:

$$\frac{\partial(\rho u_j)}{\partial x_j} = 0 \tag{1}$$

$$\frac{\partial(\rho u_i u_j)}{\partial x_j} = -\frac{\partial p}{\partial x_i} + \frac{\partial}{\partial x_j}\left(\mu\frac{\partial u_i}{\partial x_j} - \rho\overline{u'_i u'_j}\right) \tag{2}$$

where $\rho$ is the fluid density, and $x_j$ and $u_j$ are the coordinate component and velocity component in the $j$ direction, $p$ is the pressure, $\mu$ is the fluid kinematic viscosity, is the turbulent stress.

### ***Low-Re $k-\varepsilon$ models***

For laminar flow, the turbulent stress in Eq. 2 is zero. When turbulence must be considered, the turbulent stress can be described as

$$-\rho\overline{u'_i u'_j} = \mu_t\left(\frac{\partial u_i}{\partial x_j} + \frac{\partial u_j}{\partial x_i}\right) - \frac{2}{3}\rho k\delta_{ij} \tag{3}$$

where $k$ is the turbulent kinetic energy, $\mu_t$ is the turbulent eddy viscosity.

For laboratory scale reactors, the near-wall turbulence is of great importance because of low Reynolds number. Therefore, low-Re $k-\varepsilon$ models are used to describe the turbulence effect. The transport equations of turbulent kinetic energy and its dissipation rate are written as follows

$$\frac{\partial(\rho u_j k)}{\partial x_j} = \frac{\partial}{\partial x_j}\left[\left(\mu + \frac{\mu_t}{\sigma_k}\right)\frac{\partial k}{\partial x_j}\right] + G_k - \rho\varepsilon - \rho D \tag{4}$$

$$\frac{\partial(\rho u_j \varepsilon)}{\partial x_j} = \frac{\partial}{\partial x_j}\left[\left(\mu + \frac{\mu_t}{\sigma_\varepsilon}\right)\frac{\partial \varepsilon}{\partial x_j}\right] + C_{\varepsilon 1} f_1 \frac{\varepsilon}{k} G_k - C_{\varepsilon 2} f_2 \rho \frac{\varepsilon^2}{k} + E \tag{5}$$

with

$$\mu_t = C_\mu \rho f_\mu \frac{k^2}{\varepsilon} \tag{6}$$

where $C_\mu$, $\sigma_k$ and $\sigma_\varepsilon$ are empirical constants, $\varepsilon$ is the turbulent dissipation rate, $f_\mu$, $f_1$ and $f_2$ are dumping functions. $D$ and $E$ are near-wall correction terms for $k$ and $\varepsilon$ equations.

Several low-Re $k-\varepsilon$ models have been developed, which are designated as ABID for Abid [24], LB for Lam and Bremhost [25], LS for Launder and Sharma [26], YS for Yang and Shih [27], AKN for Abe and Kondoh [28] and CHC for Hsieh and Chang [29]. Damping functions for these low-Re $k-\varepsilon$ turbulence models are listed in Table 1.

### ***Degradation equation of pollutants***

Ethylene is selected as the model pollutant. After

entering the differential reactor, ethylene moves by the convection and diffusion. The governing equation of ethylene in the reactor is expressed by:

Table 1. Damping functions in turbulence models

| Model | $f_\mu$ | $f_1$ | $f_2$ |
|---|---|---|---|
| ABID | $\tanh(0.008Re_y)(1+\frac{4}{Re_t^{3/4}})$ | 1.0 | $[1-\frac{2}{9}\exp(-\frac{Re_t^2}{36})][1-\exp(-\frac{Re_y}{12})]$ |
| LB | $[1-\exp(-0.0165Re_y^2)]^2(1+\frac{20.5}{Re_t})$ | 1.0 | $1-\exp(-Re_t^2)$ |
| LS | $\exp(-\frac{3.4}{(1+Re_t/50)^2})$ | 1.0 | $1-0.3\exp(-Re_t^2)$ |
| YS | $[1-\exp(-1.5\times10^{-4}Re_y-5.0\times10^{-7}Re_y^3-1.0\times10^{-10}Re_y^5)]^{1/2}$ | $\frac{\sqrt{Re_t}}{1+\sqrt{Re}}$ | $\frac{\sqrt{Re_t}}{1+\sqrt{Re_t}}$ |
| AKN | $[1+\frac{5}{Re_t^{0.75}}\exp(-(\frac{Re_t}{200})^2)][1-\exp(-\frac{y^*}{14})]^2$ | 1.0 | $[1-0.3\exp\left(-(\frac{Re_t}{6.5})^2\right)][1-\exp(-\frac{y^*}{3.1})]^2$ |
| CHC | $[1-\exp(-0.0215Re_y)]^2(1+\frac{31.66}{Re_t^{5/4}})$ | 1.0 | $[1-0.01\exp(-Re_t^2)][1-\exp(-0.0631Re_y)]$ |

Note: $Re_t=\frac{k^2}{\nu\varepsilon}$, $Re_y=\frac{yk^{1/2}}{\nu}$, $y^*=\frac{y\varepsilon^{1/4}}{\nu^{3/4}}$

$$\frac{\partial}{\partial x_j}(u_jC)=\frac{\partial}{\partial x_j}\left[\left(D+\frac{\nu_t}{\sigma_t}\right)\frac{\partial C}{\partial x_j}\right] \quad (7)$$

where $C$ is the ethylene concentration, and $D$ is the molecular diffusion coefficient of ethylene in the gas phase, $\sigma_t$ is the turbulent Schmidt number, $\nu_t$ is the kinematic turbulent viscosity.

In differential reactors, catalysts are coated onto the wall of reactor. Thus, the photocatalytic oxidation of ethylene only occurs at the wall. For walls with catalyst, the boundary condition can be written as follows

$$-\left(D+\frac{\nu_t}{\sigma_t}\right)\frac{\partial C}{\partial n}=r \quad (8)$$

where n is the outward normal direction at the boundary. The photocatalytic rate is usually described using Langmuir-Hinshelwood equation as follows:

$$r=\frac{k'KC}{1+KC} \quad (9)$$

where $k$ is the rate constant, $K$ is the adsorption constant. Eqs. 8, 9 comprise the boundary condition of Eq. 7 as follows

$$-\left(D+\frac{\nu_t}{\sigma_t}\right)\frac{\partial C}{\partial n}=\frac{k'KC}{1+KC} \quad (10)$$

Eq. 10 should be realized in an iterated manner since the diffusion flux of ethylene to the wall changes during iteration.

For walls without catalyst, there exists

$$-\left(D+\frac{\nu_t}{\sigma_t}\right)\frac{\partial C}{\partial n}=0 \quad (11)$$

which means that no ethylene can penetrate into the wall.

***Numerical simulation***

A rectangular reactor with the dimensions of 54.5 mm × 54.5 mm × 47.5 mm is studied, as shown in Fig. 1. A glass plate with a square hollow is positioned on the bottom of reactor. Catalysts are coated onto the bottom of hollow. Polluted gas enters into the reactor and is oxidized at the surface of catalyst. Some researchers measured the degradation efficiencies under different inlet flow rates and inlet concentrations [20] . ANSYS ICEM is used to discretize the computational domain, as shown in Fig. 2. Near the surface of catalyst, the grid is refined. The total number of mesh is 565,392.

The governing equations are solved by using ANSYS Fluent. SIMPLE algorithm is adopted to deal with pressure-velocity coupling. Convection terms are discretized by using the second- order upwind scheme. The concentration equation is described by using user defined scalar (UDS). The solution was considered convergent when the scaled residuals for all equations are less than $10^{-6}$.

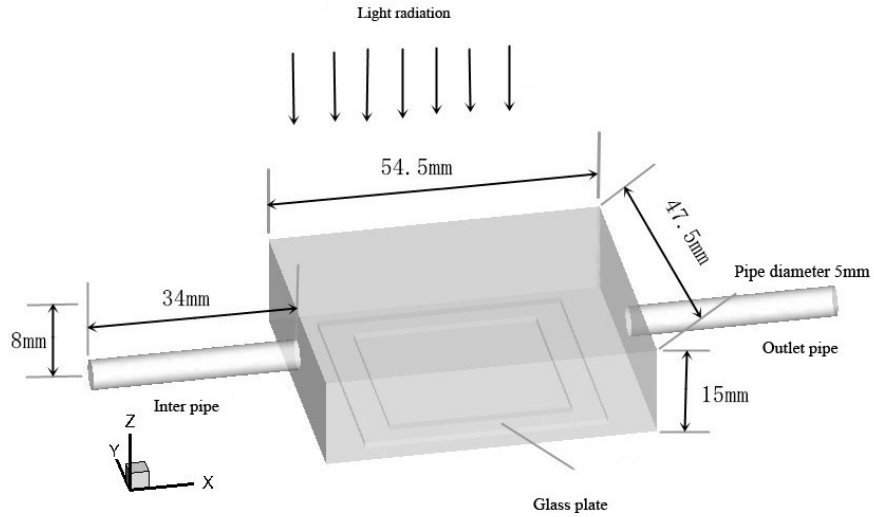


Fig. 1. Schematic of differential reactor

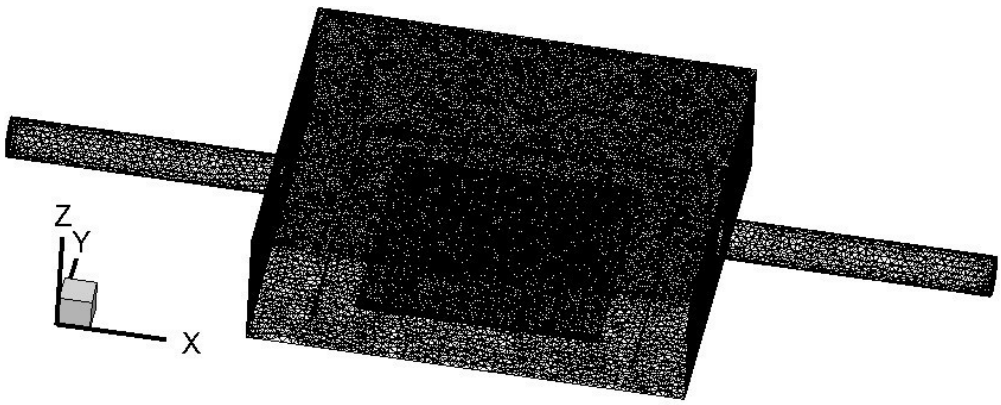


Fig. 2. Schematic of grid

At the inlet, volumetric flow rate and the concentration of pollutant are given. The selected inlet flow rates are 50 mL/min, 100 mL/min, 150 mL/min and 250 mL /min and the corresponding Reynolds numbers are 14.5, 29.0, 43.6 and 72.6, respectively. The turbulence intensity is set as 10 %. Inlet concentrations of ethylene are set as $2.11\times10^{-6}$, $4.17\times10^{-6}$, $8.33\times10^{-6}$, $1.23\times10^{-6}$ and $1.63\times10^{-6}$ mol/L, respectively. At the outlet, pressure is specified. No-slip condition is specified at all walls.

## Results and discussion

### *Velocity distribution*

Fig. 3 shows the distribution of gas velocity for laminar flow. After gas enters the reactor, vortices are formed beside two side walls of reactor, which is typical of a sudden expansion flow. In the central part of the reactor, velocities depict a uniform feature. Near the reactor outlet, the flow depicts a feature of sudden contraction. With the increase in flow rate, the vortices increase in magnitude. The vortex is restricted in a small region for 50 mL $min^{-1}$ whereas distributes full of the entire reactor cross-section for 250 mL $min^{-1}$. The velocity distributes more uniformly when the flow rate is low. Along the direction from inlet to outlet, the velocity is largest, meaning that the flow tends to be directed to the outlet. This is because the fluid is affected by the viscous stress at the wall while the shear stress at the center line is very small.

Fig. 4 shows the velocity at the center line from inlet to outlet. As shown in Fig. 4(a), When gas enters the reactor at a flow rate of 50 mL/min, the velocity is 0.0428 m/s with an error 0.9%. The maximum velocity at the center of the pipeline can reach 0.0795 m/s, which is about twice the averaged velocity. The distribution of velocity in the reactor is very non-uniform. Fig. 4(b) shows that the velocity is largest at the center of pipe, and gradually decreases toward the pipe wall, presenting a symmetrical distribution. The velocity under other flow rates are similar to each other.

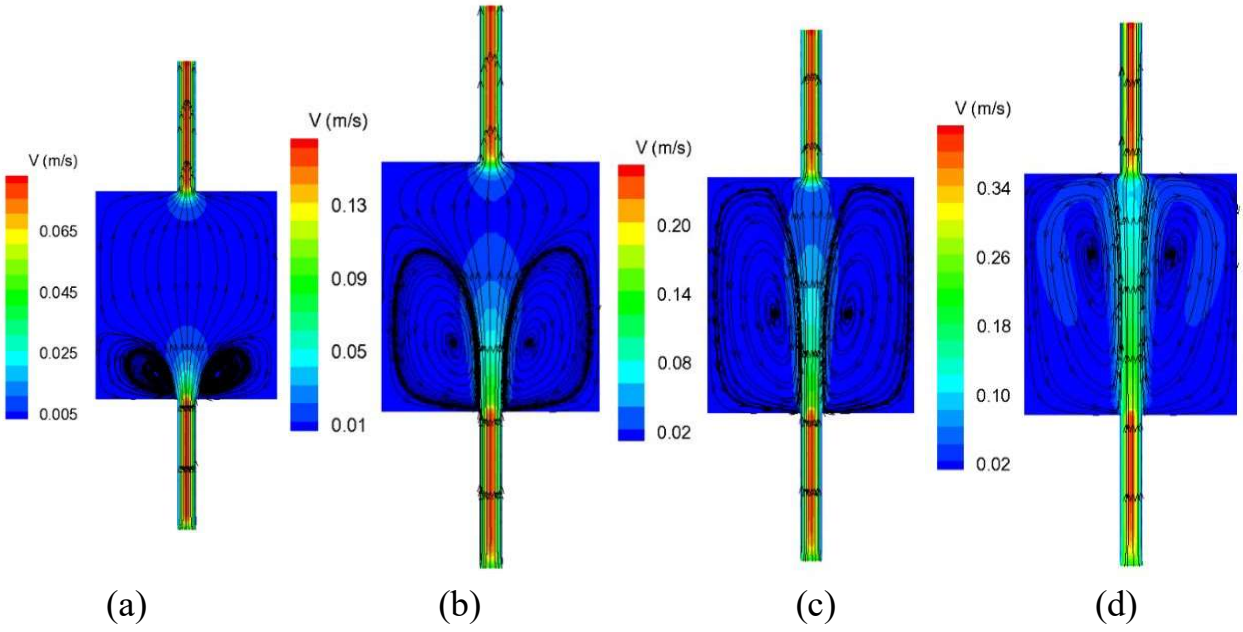


Fig. 3. Velocity distribution for laminar model at the plane of $z$=−0.5 mm: (a) 50 mL/min, (b) mL/min, (c) 150 mL/min, (d) 250 mL/min

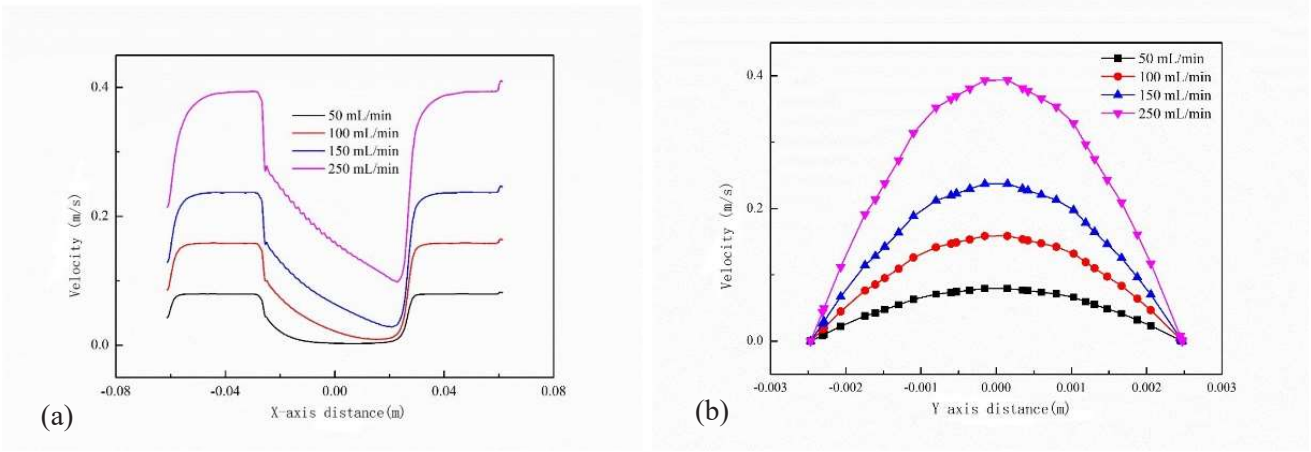


Fig. 4. Velocity profile of laminar model:
(a) (y=0, $z$=−0.5 mm), (b) ($x$=50 mm, $z$= −0.5 mm)

Fig. 5 shows the distribution of gas velocity by using the AKN low-Re $k$−$\varepsilon$ model, respectively. For 50 mL/min, vortices occupy a half of the cross-section in the reactor, which is greater than that for laminar flow. Correspondingly, the region with uniform velocity is small. The flow patterns for 250 mL/min are similar for laminar flow and two turbulence models. The velocity distributions for other low-Re $k$ − $\varepsilon$ models are similar to those of the AKN models and will not be described in detail here.

Fig. 6 shows the velocity profile at the center line from inlet to outlet. When flow rates are small, the velocity obtained by six low-Re $k$ − $\varepsilon$ model are basically consistent. As the flow rate increases, the fluid velocity also gradually increases and the velocity distributions of the six low Reynolds number models at the outlet pipe are different. When the flow rate reaches 250 mL/min, LS, YS and AKN models obtain nearly the same velocity distribution inside the reactor.

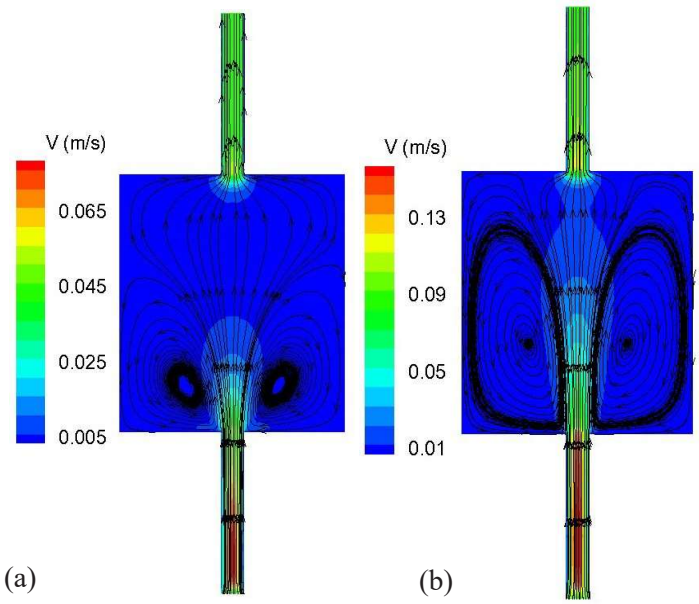


Fig. 5. Velocity distribution for the AKN model at the plane of $z$ = −0.5 mm:
(a) 50 mL/min, (b) 250 mL/min

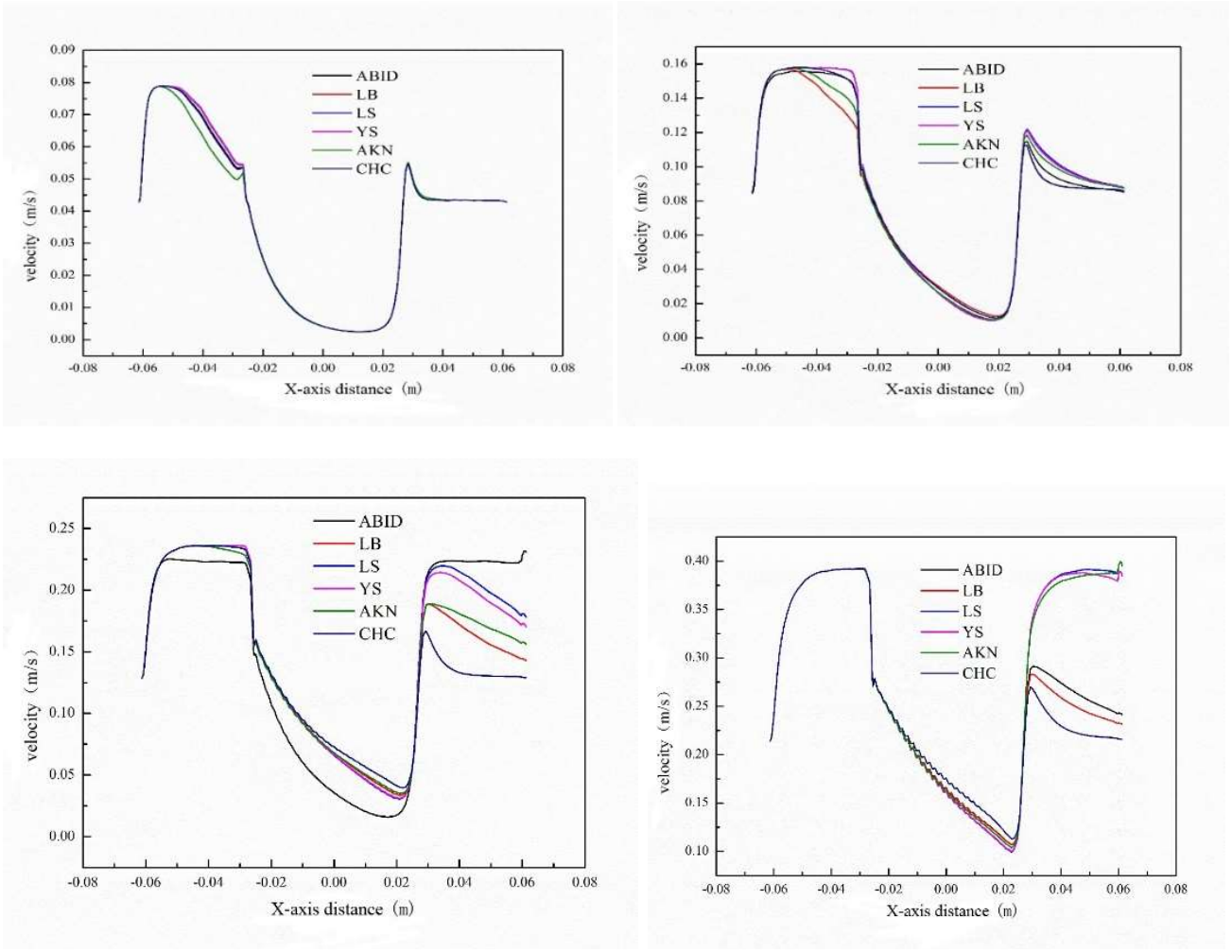


Fig. 6. Velocity profile at the position of (y = 0, *z* = −0.5 mm):
(a) 50 mL/min, (b) 100 mL/min, (c) 150 mL/min, (d) 250 mL/min

***Degradation efficiency***

Degradation efficiency is an important index to evaluate numerical simulations, which reflects the integrated effects of flow and photocatalytic reaction in differential reactors. Table 2 and Table 3 show the degradation efficiencies under different inlet concentrations for inlet flow rates of 50 mL/min and 250 mL/min, respectively. The experimental values from some researchers are also included in these two tables. For the inlet flow rates of 50 [20], all numerical simulations obtained the nearly identical result [20]. The maximum relative error appears at a low inlet concentration of 50 ppm. With the increase in inlet concentrations, the relative error decreases. The same tendency is observed for the inlet flow rates of 250 mL/min. In general, degradation efficiencies obtained by numerical simulation are consistent with the experimental values. All low-Re turbulence models behave better for small inlet concentrations whereas the laminar model predicts the better result for big inlet concentrations. In terms of degradation efficiency, all these models can be used to simulate pollutant degradation in the present photocatalytic reactor.

Table 2. Degradation efficiency under different models at 50 mL/min (%)

| ethylene concentration (ppm) | 50 | 100 | 200 | 300 | 400 |
|---|---|---|---|---|---|
| experimental value | 30.40 | 21.92 | 12.07 | 9.85 | 8.03 |
| Laminar | 23.22 | 17.51 | 11.28 | 8.37 | 6.75 |
| ABID | 23.69 | 17.63 | 11.32 | 8.37 | 6.61 |
| LB | 23.70 | 17.63 | 11.32 | 8.37 | 6.61 |
| LS | 23.70 | 17.63 | 11.32 | 8.37 | 6.61 |
| YS | 23.70 | 17.63 | 11.32 | 8.37 | 6.61 |
| AKN | 23.71 | 17.63 | 11.32 | 8.37 | 6.61 |
| CHC | 23.70 | 17.63 | 11.32 | 8.37 | 6.61 |

Table 3. Degradation efficiency under different models at 250 mL $min^{-1}$(%)

| ethylene concentration (ppm) | 50 | 100 | 200 | 300 | 400 |
|---|---|---|---|---|---|
| experimental value | 7.10 | 4.68 | 2.44 | 1.85 | 1.50 |
| Laminar | 5.02 | 3.62 | 2.29 | 1.71 | 1.35 |
| ABID | 5.19 | 3.69 | 2.30 | 1.69 | 1.33 |
| LB | 5.19 | 3.69 | 2.30 | 1.69 | 1.33 |
| LS | 5.19 | 3.69 | 2.30 | 1.69 | 1.33 |
| YS | 5.19 | 3.69 | 2.30 | 1.69 | 1.33 |
| AKN | 5.19 | 3.69 | 2.30 | 1.69 | 1.33 |
| CHC | 5.21 | 3.70 | 2.30 | 1.69 | 1.33 |

The rate constants of ethylene are fitted directly by using Eq. 9 [20]. The estimated values are $k = 1.3 \times 10^{-2}$ mol/ $ms^2$ and $K$=480 $m^3$/ mol. Fig. 7 shows the degradation efficiency for laminar flow using these rate constants. In general, the computed degradation efficiency accords well with the experimental values. However, there exists some discrepancy for small inlet flow rates. This error can be reduced by optimizing the reaction rate constant. The optimized values of $k$ and $k$ are $1.52 \times 10^{-2}$ mol/$ms^2$, and 630.0 $m^3$/mol. As shown in Fig. 8, the laminar model reproduces the experiment for both 50 mL/min and 250 mL/min using the optimized parameters.

## Conclusion

Numerical simulations of flow and reaction in differential reactors are conducted based on laminar flow and six low Re turbulence models. All simulations obtain similar flow fields. The flow in reactors is governed by vortex near the inlet. The vortex regions differ much for low inlet flow rate whereas are similar for high inlet flow rates. The degradation of ethylene is considered. The degradation efficiencies predicted by all simulations are in accordance with the experimental values. The optimization of rate constants may improve the simulation. Considering the computation complexity, laminar flow can be recommended to simulate the photocatalytic reaction in differential reactors.

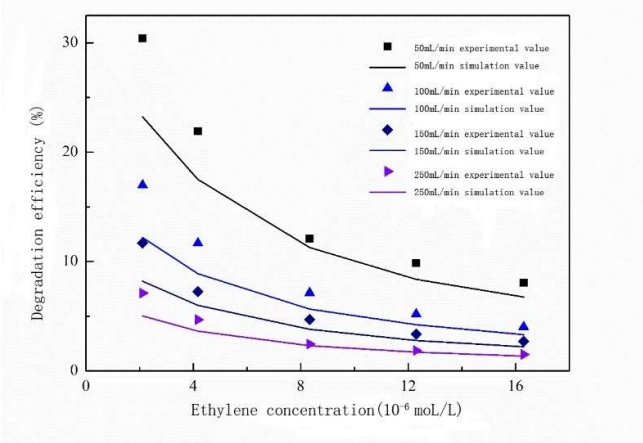


Fig. 7. Degradation efficiency of ethylene for laminar model

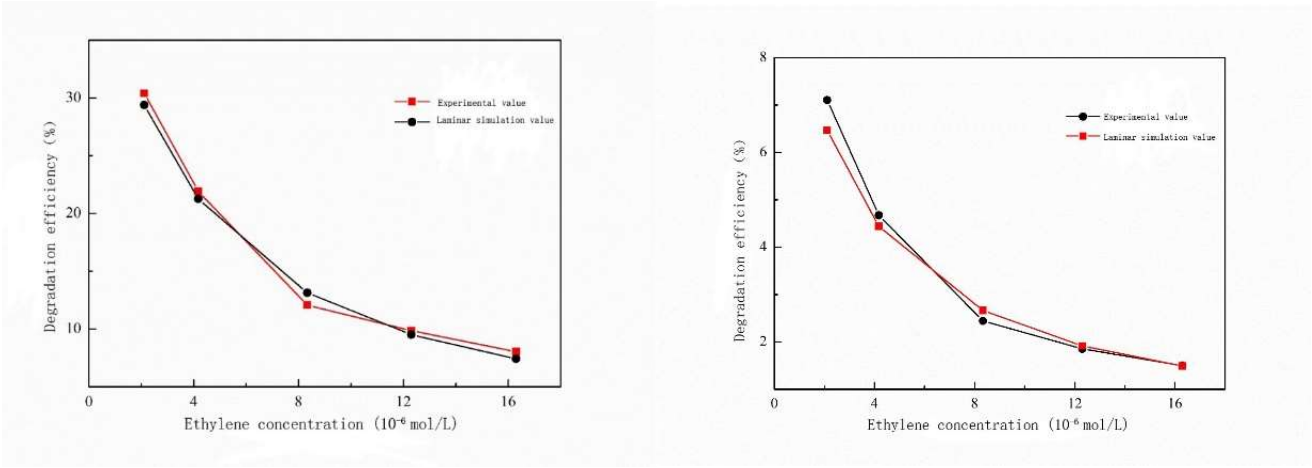


Fig. 8. Degradation efficiency of ethylene for laminar model with optimized parameters: (a) 50 mL/min, (b) 250 mL/min

**Financial supports**

The authors would like to thank the financial support by Natural Science Foundation of Shanghai (No. 17ZR1419200).

**Competing interests**

The authors declare that there are no competing interests.

**Acknowledgements**

We would like to thank Prof. Fei Chang in Department of Environmental Science and Engineering for his insight on this project.

**Ethical considerations**

"Ethical issues (Including plagiarism, Informed Consent, misconduct, data fabrication and/or falsification, double publication and/or submission, redundancy, etc.) have been completely observed by the authors."

**References**

1. AlSalka Y, Hakki A, Fleisch M, Bahnemann D. W. Understanding the degradation pathways of oxalic acid in different photocatalytic systems: Towards simultaneous photo- catalytic hydrogen evolution. Journal of Photochemistry and Photobiology A: Chemistry 2018;366:81–90.
2. Deng Y. Developing a Langmuir-type excitation equi-

librium equation to describe the effect of light intensity on the kinetics of the photocatalytic oxidation. Chemical Engineering Journal 2018;337:220 –227.
3. Chong M. N, Lei S, Jin B, Saint C, Chow C. W. Optimisation of an annular photoreactor process for degradation of Congo Red using a newly synthesized titania im- pregnated kaolinite nano-photocatalyst. Separation and Purification Technology 2009;67 (3):355–363.
4. Herrmann J. M. Photocatalysis fundamentals revisited to avoid several misconceptions. Applied Catalysis B: Environmental 2010;99 (3-4):461–468.
5. Sun X, Yan L, Xu R, Xu M, Zhu Y. Surface modification of TiO2 with poly- dopamine and its effect on photocatalytic degradation mechanism. Colloids and Surfaces A: Physicochemical and Engineering Aspects 2019;570:199–209.
6. Mohseni M, Taghipour F. Experimental and CFD analysis of photocatalytic gas phase vinyl chloride (VC) oxidation. Chemical Engineering Science 2004;59 (7):1601 –1609.
7. Vincent G, Schaer E, Marquaire P. M, Zahraa O. CFD modelling of an annu- lar reactor, application to the photocatalytic degradation of acetone. Process Safety and Environmental Protection 2011;89 (1):35–40.
8. Khodadadian F, Boer M. W. de, Poursaeidesfahani A, Van Ommen, J. R, Stankiewicz A. I., and Lakerveld, R. Design, characterization and model validation of a LED-based pho- tocatalytic reactor for gas phase applications. Chemical Engineering Journal 2018;333:456–466.
9. Duran J. E, Taghipour F, Mohseni M. CFD modeling of mass transfer in annular reactors. International Journal of Heat and Mass Transfer 2009;52 (23):5390 –5401.
10. Long F, Deng B, Xu Y, Gao J, Zhang Y. Numerical simulation of the disinfection performance in an annular reactor with different internal configurations. Journal of Water Process Engineering 2019;31:100824.
11. Wang X, Tan X, Yu T. Modeling of Formaldehyde Photocatalytic Degradation in a Honeycomb Monolith Reactor Using Computational Fluid Dynamics. Industrial & Engineering Chemistry Research 2014;53 (48):18402–18410.
12. Passal´ıa C, Alfano O, M, Brandi R. Journal Modeling and Experimental Verification of a Corrugated Plate Photocatalytic Reactor Using Computational Fluid Dynamics. Industrial & Engineering Chemistry Research 2011;50 (15):9077–9086.
13. Van Walsem J, Verbruggen S.W, Modde B, Lenaerts S, Denys S. CFD investigation of a multi-tube photocatalytic reactor in non-steady-state conditions. Chemical Engineering Journal 2016;304:808–816.
14. Wang J, Deng B, Gao J, Cao H. Numerical simulation of radiation distribution in a slurry reactor: The effect of distribution of catalyst particles. Chemical Engineering Journal 2019;357:169 –179.
15. PareekV.K, Cox S.J, Brungs M.P, Young B, Adesina A. A. Computational fluid dynamic (CFD) simulation of a pilot-scale annular bubble column photocatalytic reactor. Chemical Engineering Science 2003;58 (3-6):859–865.
16. Boyjoo Y, Ang M, Pareek V. CFD simulation of a pilot scale slurry photocatalytic reactor and design of multiple-lamp reactors. Chemical Engineering Science 2014;111:266– 277.
17. Bagheri M, Mohseni M. Computational fluid dynamics (CFD) modeling of VUV/UV photoreactors for water treatment. Chemical Engineering Journal 2014;256:51 –60.
18. Elyasi S, Taghipour F. Simulation of UV photoreactor for water disinfection in Eu- lerian framework. Chemical Engineering Science 2006;61 (14):4741 –4749.
19. Casado C, Marug´an J, Timmers R, Mun˜oz M, Grieken R. van. Comprehen- sive multiphysics modeling of photocatalytic processes by computational fluid dynamics based on intrinsic kinetic parameters determined in a differential photoreactor. Chemical Engineering Journal 2017;310:368 –380.
20. Einaga H, Tokura J, Teraoka Y, Ito K. Kinetic analysis of TiO2-catalyzed hetero- geneous photocatalytic oxidation of ethylene using computational fluid dynamics. Chemical Engineering Journal 2015;263:325–335.
21. Motegh M, Cen J, Appel P.W, Ommen J.R.Van, Kreutzer M.T. Photocatalytic- reactor efficiencies and simplified expressions to assess their relevance in kinetic experi- ments. Chemical Engineering Journal 2012;207-208:607 –615.
22. TaghipourF, Mohseni M. CFD simulation of UV photocatalytic reactors for air treatment. AIChE Journal 2005;51 (11):3039–3047.
23. Verbruggen S.W, Lenaerts, S, Denys S. Analytic versus CFD approach for kinetic modeling of gas phase photocatalysis. Chemical Engineering Journal 2015;262:1–8.
24. Abid R. Evaluation of two-equation turbulence models for predicting transitional flows. International Journal of Engineering Science 1993;31 (6):831–840.
25. Lam C, Bremhost K. A Modified Form of the k-e Model for Predicting Wall Turbu- lence. Journal of Fluids Engineering 1981;103:456–460.
26. Launder B. E, Sharma B. I. Application of the energy-dissipation model of turbulence to the calculation of flow near a spinning disc. Letters in Heat and Mass Transfer 1974;1:131–138.
27. Yang Z, Shih T. H. New time scale based k-epsilon model for near-wall turbulence. AIAA Journal 1993;31 (7):1191–1198.
28. AbeK, Kondoh, T. A new turbulence model for predicting fluid flow and heat transfer in separating and reattaching flows-l. Flow field calculations. International Journal of Heat and Mass Transfer 1994;37 (1):139–151.
29. Hsieh W., Chang K. C. Calculation of wall heat transfer in pipe-expansion turbulent flows. International Journal of Heat and Mass Transfer 1996;39:1831–3822.